


Research Article

A Novel Microscopic Modeling Scheme for the Shape Memory Polymer Composites with respect to the Ambient Temperature

Yang Li,¹ Junjie Ye ,² Lu Liu,² Baoquan Shi,² and Yumin He³

¹*Xi'an Institute of Space Radio Technology, Xi'an 710100, China*

²*Research Center for Applied Mechanics, Key Laboratory of Ministry of Education for Electronic Equipment Structure Design, Xidian University, Xi'an 710071, China*

³*College of Mechanical and Electrical Engineering, Xi'an University of Architecture and Technology, Xi'an 710055, China*

Correspondence should be addressed to Junjie Ye; ronkey6000@sina.com

Received 10 March 2022; Revised 18 April 2022; Accepted 27 June 2022; Published 22 July 2022

Academic Editor: Chuang Liu

Copyright © 2022 Yang Li et al. This is an open access article distributed under the Creative Commons Attribution License, which permits unrestricted use, distribution, and reproduction in any medium, provided the original work is properly cited.

This paper is aimed at studying the effective mechanical property of shape memory polymer composites (SMPC) reinforced with natural short fibers. To this end, a novel modeling scheme was presented. The SMPC was firstly equivalent to the composite laminates, and the natural short fibers are also subtly equivalent to the ellipsoidal inclusions distributed in the matrix materials periodically. Moreover, a represented volume element along laminate thickness can be easily chosen, and its elastic constants are accurately acquired by employing a proper microscopic mechanical model. Herein, the high-fidelity generalized method of cells, which represents a good ability in predicting the effective mechanical behaviors of composites, was used. On this basis, the classic laminate theory was improved to suitable for describing the elastic constants and failure strength the SMPC with respect to ambient temperature. Numerical results show a good consistency to the experimental data. Moreover, a higher ambient temperature tends to sharply decrease their final failure strength. It is also revealed that the presented modeling method shows a great potential in calculating the effectively mechanical property of the natural short fiber-reinforced composites.

1. Introduction

Due to its unique molecular structure and good performances, including light weight, low cost, and high strain recovery rate, shape memory polymer (SMP) exhibits a widespread prospect in medical, energy, and electronic communications [1, 2]. It is reported by Leng et al. [3] that the maximum strain of the SMP reach to 600%. However, its low stiffness and recovery stress seriously limited its application in some extent. To overcome the flaws mentioned above, some reinforced phases, such as carbon fibers, carbon nanotubes, and nanoparticle, were presented to be mixed with the SMP to form the shape memory polymer composites (SMPC) [4]. Due to its intrinsic characteristic of the slow unfolding, the SMPC have been widely prepared as some deployable components in the satellite equipment, such as hinge and truss structure [5]. According to a statistical result by Castet and Saleh [6], the failure of solar wing during the deployment procedure is accounting for 17% of the total fail-

ure events, which results in a final failure of the satellite. To maximum guarantee the safe operation of the satellite equipment, it is critical to grasp the effective mechanical property of the SMPC with respect to the ambient temperature.

A large number of experimental tests have been executed on the standard specimen or structure of the SMPC to acquire its mechanical [7–9], electrical [10, 11], and shape memory performances [12]. The recovery capable of the SMPC under various loads was investigated by Basit et al. [13], and it exhibits a good potential in diverse applications. Le and Goo [14] executed on a folding and deployment test of the SMPC hinge at -10°C to investigate its shape recoverability and revealed that its deployment performance is closely dependent on ambient temperature. To reveal the temperature influences, an infrared camera and thermocouples were employed to observe the temperature distribution. By using a series of experimental methods, Wang et al. [15] studied the thermodynamic and shape memory properties of the SMPC. Moreover, its fracture interface was investigated

by scanning electron microscopy. It is indicated that a good mechanical property can be acquired when fiber mass fraction is equal to 8%. Dao et al. [16, 17] measured the moment and blocking force of the SMPC hinge by employing a pulley-mass system. The test method provides a guideline for evaluating its mechanical performances. Annin et al. [18] investigated the deformation and damage of the SMPC during the bending and torsion. Moreover, the fiber off-axis angle influences on the formation process was also revealed. Lelieveld et al. [19] executed on the thermomechanical tests to investigate the actuation characteristics of the SMPC. Kim et al. [20] explored the recovery and physical properties by using the experimental tests on the strength and thermal conductivity.

In recent years, a large number of theoretical methods [21] have been presented to investigate elastic constants, nonlinear deformation, and failure characteristic of the SMPC. With an analogy way with thermomechanical responses at macroscale, Wang et al. [22] presented a chain model to optimize the chain system of the SMPC. It is revealed that the shape memory property is improved by increasing the cross link density. Arvanitakis [23] presented a constitutive level-set model to capture its mechanical behaviors under the thermomechanical cycle loading. Sun et al. and Gu et al. [24, 25] presented a multiscale strategy and established the thermoviscoelastic constitutive equation to investigate the buckling critical stress under the finite deformation, and the numerical results lay a solid foundation for its application and design. Bergman and Yang [26] proposed a macroscopic model combining a nonlinear geometric model with a temperature-dependent constitutive equation to investigate the shape fixation process. Li et al. [27] established a three dimension model by employing the ABAQUS to study the vibration mode and natural frequency of the large spatial deployable structure. The modal test results show a good consistency with the simulation results. Based on the homogenization scheme, Song et al. [28] presented a constitutive model for the SMPC subjected to the thermomechanical load. The experimental tests were executed on the standard specimens for a comparison.

For the SMPC, the mechanical property is closely dependent on its microscopic feature, including inclusion arrangement, interfacial bonding, and inclusion morphology. It is hardly for a macroscopic model to reveal the microscopic characteristic influences. A comprehensive investigation with full consideration of the microscopic factors influence has been executed by some researchers. By choosing a cylindrical representative volume element (RVE), Khalili et al. [29] evaluated the interface property influences on mechanical behaviors of the SMPC. Liu and Jiang [30] presented a novel hierarchical micromechanic method to study the microstructural feature influences on the thermal conducting behavior of the SMPC. However, few studies refer to random inclusions in the matrix materials. The main objective of this paper is to focus on investigating the effective mechanical property of the SMP reinforced with natural short fibers. To this end, an effective modeling scheme based on the microscopic constitutive equation was presented. The outline was summarized as follows: Section 2 presented the

modeling scheme and microscopic modeling process of the SMP reinforced with natural short fibers. To validate the effectiveness of the presented method, experimental data and numerical results were both introduced for a comparison in Section 3. On this basis, a series of simulation analysis were executed to fully study the failure strength of the SMPC with respect to ambient temperature in Section 4. Conclusions are shown in Section 5.

2. Modeling Process of the SMPC

2.1. The Equivalent Procedure of the SMPC. For the shape memory polymer composites, short fibers always present obvious random characteristic due to the limitation of the preparation technology as shown in Figure 1(a). In the coordinate system $x_1-x_2-x_3$, the short fiber direction can be accurately determined with respect to the fiber angles of θ and γ as shown in Figure 1(b).

It is reported by Cai et al. [31, 32] that the random short fibers exhibit an obvious directionality and closely dependent on resin flow direction. To simplify the microscopic modeling procedure, the random short fibers are always considered to be periodically distributed in matrix materials according to the homogenization theory as shown in Figure 2(a). According to the statistical results derived from the microscopic morphology, the random short fibers are equivalently represented by the ellipsoidal model. In addition, the fiber direction and density along thickness direction represent obvious differences. In details, few fibers can be found in the upper and lower edges, and the short fiber density in the center location is much higher. Therefore, the equivalent structure of the SMPC can be considered as the composite laminate (Figure 2(b)), whose upper and lower edges consist of pure polymer, while other regions can be treated as serials of unidirectional (UD) laminas. To sum up, the SMPC are accurately discretized as ten UD laminas, and eight of them are reinforced with ellipsoidal fibers. It should be noted that the elastic modulus of the natural fiber composites along x_1 -direction is identical to the equivalent composites.

2.2. Numerical Modeling Process. It is assumed that the SMPC is equivalent to the composite laminates, which consist of serials of the UD laminas mentioned above. The equivalent ellipsoidal inclusions are assumed to be periodically distributed in the SMP. The simplified numerical procedure for the SMPC can be summarized as follows: (1) a proper RVE in each lamina can be easily selected along the thickness direction as shown in Figure 2(c). On this basis, the effective modulus of each lamina can be obtained by employing an effective microscopic mechanical model. (2) The SMPC consists of a series of unidirectional laminas. Therefore, the effective elastic modulus and mechanical property of the SMPC can be acquired by employing the classic laminate theory. (3) The numerical results by the presented method and experimental data are both employed for a comparison. On this basis, the failure strength of the SMPC with respect to ambient temperature is investigated by implanted the failure criterion.

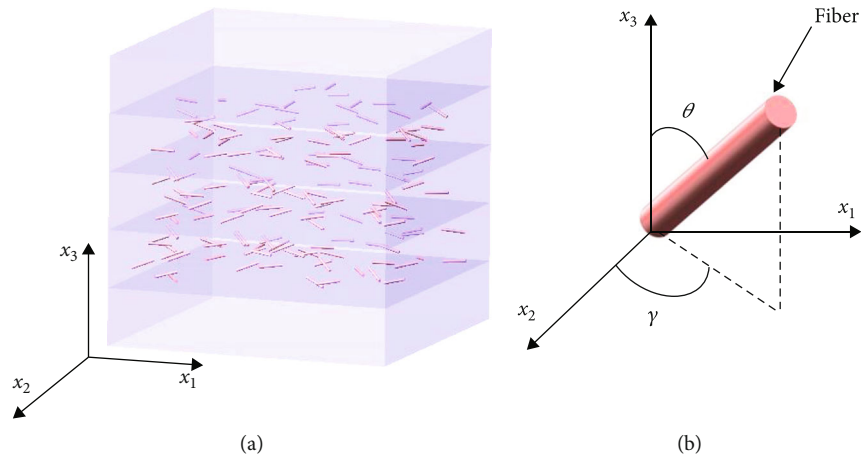


FIGURE 1: Three-dimension image of the SMPC. (a) SMPC reinforced with short fibers. (b) Short fiber direction.

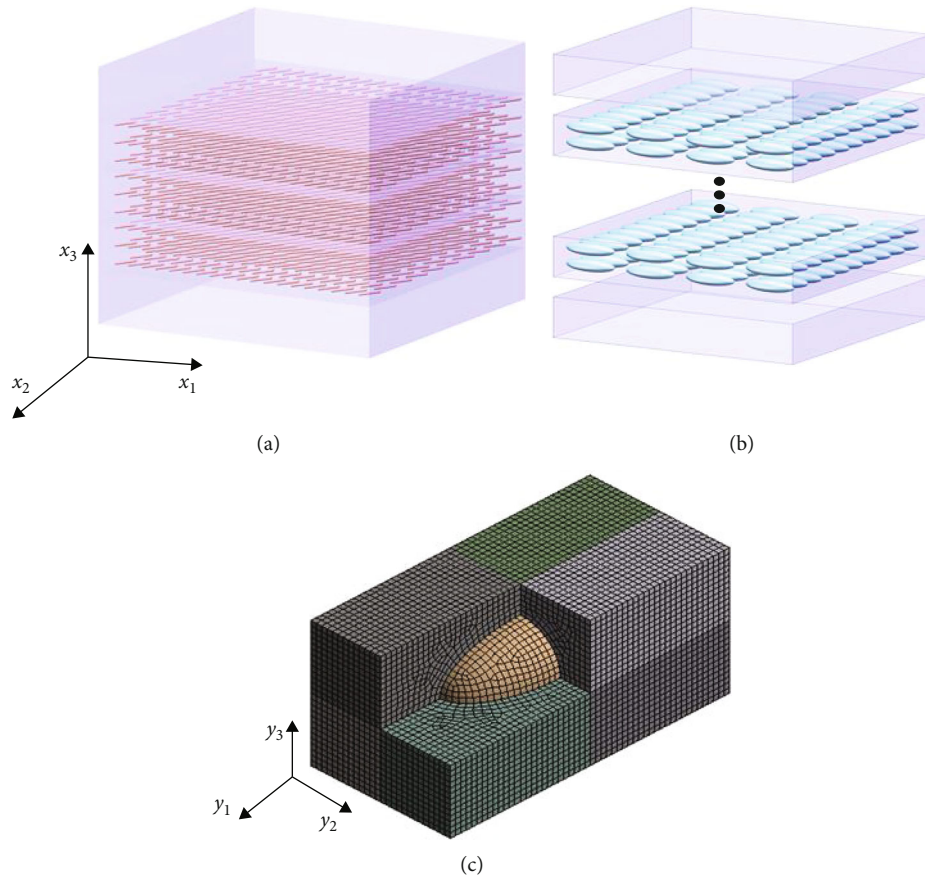


FIGURE 2: Simplified modeling procedure of the SMPC reinforced with natural short fibers. (a) The effective 3D equivalent structure. (b) SMPC treated as the composite laminated reinforced with the periodic ellipsoidal inclusion. (c) The RVE discretized by serials of hexahedral subcells.

2.2.1. Microscopic Constitutive Relation. By employing a microscopic mechanical theory, such as Eshelby equivalent inclusion theory [33], Mori-Tanaka method [34], self-consistent model, and generalized self-consistent model [35], the elastic constants of the composites can be acquired. However, they limit to analyze some inclusions with special geometric shape. It is hardly for the microscopic theories mentioned above to reveal the relation between geometric

shape and inclusion distribution influences on the effective modulus. In recent years, the high-fidelity generalized method of cells (HFGMC) represented a good ability to investigate nonlinear deformation [36] and failure modes [37] of the composites under a coupled multifield environment. Ye et al. [38] presented a multiscale modeling framework by combining with the finite element method (FEM) to reveal the failure mechanism of the composites from

microscopic damage to macroscopic fracture. Herein, the HFGMC is employed to calculate the effective modulus of the RVE reinforced with a spheroidal inclusion. During the numerical modeling process, the RVE as shown in Figure 2(c) is discretized as $N_\alpha \times N_\beta \times N_\gamma$ subcells. It should be noted that the parameters N_α , N_β , and N_γ indicate the discretized subcell number along y_1 -, y_2 -, and y_3 -direction, respectively. The subscripts $\alpha = 1, 2, \dots, N_\alpha$, $\beta = 1, 2, \dots, N_\beta$, and $\gamma = 1, 2, \dots, N_\gamma$ indicate the numbered subcell. The second-order subcell displacement component $u_i^{(\alpha\beta\gamma)}$ in the RVE is expressed as the function of the fluctuating average displacements $W_{i(000)}^{(\alpha\beta\gamma)}$ and the higher-order displacement components $W_{i(lmn)}^{(\alpha\beta\gamma)}$, that is,

$$\begin{aligned} u_i^{(\alpha\beta\gamma)} = & \bar{\varepsilon}_{ij} x_j + W_{i(000)}^{(\alpha\beta\gamma)} + \bar{y}_1^{(\alpha)} W_{i(000)}^{(\alpha\beta\gamma)} + \bar{y}_2^{(\beta)} W_{i(010)}^{(\alpha\beta\gamma)} \\ & + \bar{y}_3^{(\gamma)} W_{i(001)}^{(\alpha\beta\gamma)} + \frac{1}{2} \left[3\bar{y}_1^{(\alpha)^2} - \frac{d_\alpha^2}{4} \right] W_{i(200)}^{(\alpha\beta\gamma)} \\ & + \frac{1}{2} \left[3\bar{y}_2^{(\beta)^2} - \frac{h_\beta^2}{4} \right] W_{i(020)}^{(\alpha\beta\gamma)} + \frac{1}{2} \left[3\bar{y}_3^{(\gamma)^2} - \frac{l_\gamma^2}{4} \right] W_{i(002)}^{(\alpha\beta\gamma)}, \end{aligned} \quad (1)$$

where d_α , h_β , and l_γ denote the subcell dimension along y_1 -, y_2 -, and y_3 -direction (Figure 2(c)), respectively.

With full consideration of the displacement continuity condition between the adjacent subcells, the relation between the subcell strain components $\varepsilon_{ij}^{(\alpha\beta\gamma)}$ and average strains $\bar{\varepsilon}_{ij}$ can be expressed as follows [36, 39]:

$$\sum_{\alpha=1}^{N_\alpha} d_\alpha \varepsilon_{11}^{(\alpha\beta\gamma)} = d \bar{\varepsilon}_{11} \quad (\beta = 1, \dots, N_\beta, \gamma = 1, \dots, N_\gamma), \quad (2)$$

$$\sum_{\beta=1}^{N_\beta} h_\beta \varepsilon_{22}^{(\alpha\beta\gamma)} = h \bar{\varepsilon}_{22} \quad (\alpha = 1, \dots, N_\alpha, \gamma = 1, \dots, N_\gamma), \quad (3)$$

$$\sum_{\gamma=1}^{N_\gamma} l_\gamma \varepsilon_{33}^{(\alpha\beta\gamma)} = l \bar{\varepsilon}_{33} \quad (\alpha = 1, \dots, N_\alpha, \beta = 1, \dots, N_\beta), \quad (4)$$

$$\sum_{\beta=1}^{N_\beta} \sum_{\gamma=1}^{N_\gamma} h_\beta l_\gamma \varepsilon_{23}^{(\alpha\beta\gamma)} = hl \bar{\varepsilon}_{23} \quad (\alpha = 1, \dots, N_\alpha), \quad (5)$$

$$\sum_{\alpha=1}^{N_\alpha} \sum_{\gamma=1}^{N_\gamma} d_\alpha l_\gamma \varepsilon_{13}^{(\alpha\beta\gamma)} = dl \bar{\varepsilon}_{13} \quad (\beta = 1, \dots, N_\beta), \quad (6)$$

$$\sum_{\alpha=1}^{N_\alpha} \sum_{\beta=1}^{N_\beta} d_\alpha h_\beta \varepsilon_{12}^{(\alpha\beta\gamma)} = dh \bar{\varepsilon}_{12} \quad (\gamma = 1, \dots, N_\gamma), \quad (7)$$

where the symbols d , h , and l denote the dimension of the RVE.

Similarly, the normal stress continuity between the adjacent subcells are written as:

$$\sigma_{11}^{(1\beta\gamma)} = \sigma_{11}^{(2\beta\gamma)} = \dots = \sigma_{11}^{(N_\alpha\beta\gamma)} = T_{11}^{(\beta\gamma)} \quad (\beta = 1, \dots, N_\beta, \gamma = 1, \dots, N_\gamma), \quad (8)$$

$$\sigma_{22}^{(\alpha 1\gamma)} = \sigma_{22}^{(\alpha 2\gamma)} = \dots = \sigma_{22}^{(\alpha N_\beta\gamma)} = T_{22}^{(\alpha\gamma)} \quad (\beta = 1, \dots, N_\beta, \gamma = 1, \dots, N_\gamma), \quad (9)$$

$$\sigma_{33}^{(\alpha\beta 1)} = \sigma_{33}^{(\alpha\beta 2)} = \dots = \sigma_{33}^{(\alpha\beta N_\gamma)} = T_{33}^{(\alpha\beta)} \quad (\alpha = 1, \dots, N_\alpha, \beta = 1, \dots, N_\beta), \quad (10)$$

where $\sigma_{ii}^{(\alpha\beta\gamma)}$ ($i = 1, 2, 3$) indicates subcell stress components, which can be simplified as the function of $T_{ii}^{(**)}$.

With respect to the axial symmetry characteristic, that is, $\sigma_{ij}^{(\alpha\beta\gamma)} = \sigma_{ji}^{(\alpha\beta\gamma)}$ ($i, j = 1, 2, 3$ and $i \neq j$), the sub-cell shear stress components in the α th row are expressed:

$$\sigma_{23}^{(\alpha 1\gamma)} = \sigma_{23}^{(\alpha 2\gamma)} = \dots = \sigma_{23}^{(\alpha N_\beta\gamma)} \quad (\alpha = 1, \dots, N_\alpha), \quad (11)$$

$$\sigma_{32}^{(\alpha\beta 1)} = \sigma_{32}^{(\alpha\beta 2)} = \dots = \sigma_{32}^{(\alpha\beta N_\gamma)} \quad (\alpha = 1, \dots, N_\alpha). \quad (12)$$

In the α th row, the shear stresses $\sigma_{23}^{(\alpha\beta\gamma)}$ can be simplified as follows:

$$\sigma_{23}^{(\alpha\beta\gamma)} = \sigma_{23}^{(\alpha\beta\gamma)} = \dots = T_{23}^{(\alpha)} \quad (\alpha = 1, \dots, N_\alpha). \quad (13)$$

Similarly, the shear stress components $\sigma_{13}^{(\alpha\beta\gamma)}$ and $\sigma_{13}^{(\alpha\beta\gamma)}$ can be simplified as follows:

$$\sigma_{13}^{(\alpha\beta\gamma)} = \sigma_{13}^{(\alpha\beta\gamma)} = \dots = T_{13}^{(\beta)} \quad (\beta = 1, \dots, N_\beta), \quad (14)$$

$$\sigma_{12}^{(\alpha\beta\gamma)} = \sigma_{12}^{(\alpha\beta\gamma)} = \dots = T_{12}^{(\gamma)} \quad (\gamma = 1, \dots, N_\gamma). \quad (15)$$

It is revealed that the matrix materials always represented inelastic deformation. Moreover, the thermal residual stress can be easily discerned due to the mismatch of thermal expansion coefficients between the inclusion and matrix materials. Therefore, the average subcell strain components $\bar{\varepsilon}^{(\alpha\beta\gamma)}$ in the RVE are written as the function of the subcell stress $\bar{\sigma}^{(\alpha\beta\gamma)}$, that is,

$$\bar{\varepsilon}^{(\alpha\beta\gamma)} = S^{(\alpha\beta\gamma)} \bar{\sigma}^{(\alpha\beta\gamma)} + \bar{\varepsilon}^p(\alpha\beta\gamma) + \alpha^{(\alpha\beta\gamma)} \Delta T, \quad (16)$$

where $\bar{\varepsilon}^{(\alpha\beta\gamma)}$ and $S^{(\alpha\beta\gamma)}$ represent the subcell strain and flexibility matrix, respectively. $\bar{\varepsilon}^p(\alpha\beta\gamma)$ and $\alpha^{(\alpha\beta\gamma)}$ are the subcell inelastic strain and thermal expansion coefficient. ΔT is the ambient temperature variation.

In Equation (16), the subcell thermal residual stress is determined by the temperature variation and thermal expansion coefficients of the constituent materials. Inelastic subcell strain $\bar{\varepsilon}^p(\alpha\beta\gamma)$ can be calculated according to the loading step size. It is indicated that the subcell average strain $\bar{\varepsilon}^{(\alpha\beta\gamma)}$ can be effectively calculated once the subcell averaged

stress $\bar{\sigma}^{(\alpha\beta\gamma)}$ is determined. From Equations (8)–(10) and Equations (13)–(15), the subcell normal stress and shear stress components are solved.

Substituting Equations (8)–(10) and Equations (13)–(15) into Equation (16), the subcell average strain components $\bar{\varepsilon}^{(\alpha\beta\gamma)}$ are obtained. Combining with the displacement continuity condition in Equations (2)–(7), the subcell stresses $T_{ij}^{(*)}$ can be written as matrix form, that is,

$$\begin{bmatrix} T_{11}^{(\beta\gamma)} \\ T_{22}^{(\alpha\gamma)} \\ T_{33}^{(\alpha\beta)} \\ T_{23}^{(\alpha)} \\ T_{13}^{(\beta)} \\ T_{12}^{(\gamma)} \end{bmatrix} = \mathbf{C} \begin{bmatrix} \bar{\varepsilon}_{11} \\ \bar{\varepsilon}_{22} \\ \bar{\varepsilon}_{33} \\ \bar{\varepsilon}_{23} \\ \bar{\varepsilon}_{13} \\ \bar{\varepsilon}_{12} \end{bmatrix} + \begin{bmatrix} \Theta_{11}^{(\beta\gamma)} \\ \Theta_{22}^{(\alpha\gamma)} \\ \Theta_{33}^{(\alpha\beta)} \\ \Theta_{23}^{(\alpha)} \\ \Theta_{13}^{(\beta)} \\ \Theta_{12}^{(\gamma)} \end{bmatrix} + \begin{bmatrix} \Gamma_{11}^{(\beta\gamma)} \\ \Gamma_{22}^{(\alpha\gamma)} \\ \Gamma_{33}^{(\alpha\beta)} \\ \Gamma_{23}^{(\alpha)} \\ \Gamma_{13}^{(\beta)} \\ \Gamma_{12}^{(\gamma)} \end{bmatrix} \Delta T, \quad (17)$$

where $\bar{\varepsilon}_{ij}$ and $\Theta_{ij}^{(**)}$ indicate the macroscopic average strain and inelastic stress components. $\Gamma_{ij}^{(**)}$ denotes the thermal expansion coefficients of the constituent materials. The symbol \mathbf{C} is the stiffness matrix, which consists of subcell dimension.

Once subcell stress components in Equation (17) is obtained, the macroscopic average stress $\bar{\sigma}$ can be easily solved according to the homogenization theory, given by,

$$\bar{\sigma} = \frac{1}{dhl} \sum_{\alpha=1}^{N_\alpha} \sum_{\beta=1}^{N_\beta} \sum_{\gamma=1}^{N_\gamma} d_\alpha h_\beta l_\gamma \sigma^{(\alpha\beta\gamma)}. \quad (18)$$

Substituting Equation (17) into Equation (18), the macroscopic average stress is written as the function of macroscopic average strain $\bar{\varepsilon}$ and inelastic strain $\bar{\varepsilon}^I$, that is,

$$\bar{\sigma} = \mathbf{C}^* (\bar{\varepsilon} - \bar{\varepsilon}^I - \alpha^* \Delta T), \quad (19)$$

where \mathbf{C}^* is the stiffness matrix of the composites.

2.2.2. Microscopic Constitutive Relation. Herein, the SMPC is considered to be composed of some UD laminas. Once the elastic modulus and mechanical behavior of each UD lamina are determined, the overall property of the SMPC can be obtained by employing the classic laminate theory [40, 41]. For each UD lamina, the stress-strain relation in the global coordinate system $x_1 - x_2$ with respect to inelastic strain $\bar{\varepsilon}_i^I$ and thermal strain is improved as follows:

$$\begin{bmatrix} \sigma_x \\ \sigma_y \\ \tau_{xy} \end{bmatrix} = \begin{bmatrix} \bar{Q}_{11}^k & \bar{Q}_{12}^k & \bar{Q}_{16}^k \\ \bar{Q}_{12}^k & \bar{Q}_{22}^k & \bar{Q}_{26}^k \\ \bar{Q}_{16}^k & \bar{Q}_{26}^k & \bar{Q}_{66}^k \end{bmatrix} \begin{bmatrix} \varepsilon_x^0 \\ \varepsilon_y^0 \\ \gamma_{xy}^0 \end{bmatrix} + z \begin{bmatrix} k_x \\ k_y \\ k_{xy} \end{bmatrix} - \begin{bmatrix} \varepsilon_x^I \\ \varepsilon_y^I \\ \gamma_{xy}^I \end{bmatrix} - \Delta T \begin{bmatrix} \alpha_x^k \\ \alpha_y^k \\ \alpha_{xy}^k \end{bmatrix}, \quad (20)$$

where σ_x , σ_y , and τ_{xy} indicate the stress components in the global coordinate system. ε_x^0 , ε_y^0 , and γ_{xy}^0 are the midplane strain components in the composite laminates. z and \bar{Q}_{ij}^k are the thickness and stiffness matrix of the laminate. k_x , k_y , and k_{xy} are related to the partial differentiation of displacement to the global coordinate.

The total thickness of composite laminates is consider as the sum of each UD lamina, that is,

$$H = \sum_{k=1}^N (z_k - z_{k-1}), \quad (21)$$

where the symbol N is the laminate number.

The internal force components N_x , N_y , and N_{xy} as well as the internal force moments M_x , M_y , and M_{xy} in each lamina can be acquired by executing on an integral operation along the thickness, that is,

$$\begin{bmatrix} N_x \\ N_y \\ N_{xy} \end{bmatrix} = \sum_{k=1}^N \begin{bmatrix} \bar{Q}_{11}^k & \bar{Q}_{12}^k & \bar{Q}_{16}^k \\ \bar{Q}_{12}^k & \bar{Q}_{22}^k & \bar{Q}_{26}^k \\ \bar{Q}_{16}^k & \bar{Q}_{26}^k & \bar{Q}_{66}^k \end{bmatrix} \left\{ \int_{z_{k-1}}^{z_k} \begin{bmatrix} \varepsilon_x^0 \\ \varepsilon_y^0 \\ \gamma_{xy}^0 \end{bmatrix} dz + \int_{z_{k-1}}^{z_k} z \begin{bmatrix} k_x \\ k_y \\ k_{xy} \end{bmatrix} dz - \int_{z_{k-1}}^{z_k} \begin{bmatrix} \varepsilon_x^I \\ \varepsilon_y^I \\ \gamma_{xy}^I \end{bmatrix} dz - \int_{z_{k-1}}^k \Delta T \begin{bmatrix} \alpha_x^k \\ \alpha_y^k \\ \alpha_{xy}^k \end{bmatrix} dz \right\}, \quad (22)$$

$$\begin{bmatrix} M_x \\ M_y \\ M_{xy} \end{bmatrix} = \sum_{k=1}^N \begin{bmatrix} \bar{Q}_{11}^k & \bar{Q}_{12}^k & \bar{Q}_{16}^k \\ \bar{Q}_{12}^k & \bar{Q}_{22}^k & \bar{Q}_{26}^k \\ \bar{Q}_{16}^k & \bar{Q}_{26}^k & \bar{Q}_{66}^k \end{bmatrix} \left\{ \int_{z_{k-1}}^{z_k} z \begin{bmatrix} \varepsilon_x^0 \\ \varepsilon_y^0 \\ \gamma_{xy}^0 \end{bmatrix} dz + \int_{z_{k-1}}^{z_k} z^2 \begin{bmatrix} k_x \\ k_y \\ k_{xy} \end{bmatrix} dz - \int_{z_{k-1}}^{z_k} z \begin{bmatrix} \varepsilon_x^I \\ \varepsilon_y^I \\ \gamma_{xy}^I \end{bmatrix} dz - \int_{z_{k-1}}^k \Delta T z \begin{bmatrix} \alpha_x^k \\ \alpha_y^k \\ \alpha_{xy}^k \end{bmatrix} dz \right\}, \quad (23)$$

where k_x and k_y are the bend deflection rates. k_{xy} is the distorting rate in the midplane.

It can be found that the internal strain, midplane bend deflection, and distorting rates are unrelated to the laminate

thickness. Equations (22) and (23) can be further simplified. The constitutive relation of the composite laminates with respect to inelastic strain and thermal strain components can be written as:

$$\begin{bmatrix} N_x + N_x^I + N_x^T \\ N_y + N_y^I + N_y^T \\ N_{xy} + N_{xy}^I + N_{xy}^T \\ M_x + M_x^I + M_x^T \\ M_y + M_y^I + M_y^T \\ M_{xy} + M_{xy}^I + M_{xy}^T \end{bmatrix} = \begin{bmatrix} \mathbf{A} & \mathbf{B} \\ \mathbf{B} & \mathbf{D} \end{bmatrix} \begin{bmatrix} \epsilon_x^0 \\ \epsilon_y^0 \\ \gamma_{xy}^0 \\ k_x \\ k_y \\ k_{xy} \end{bmatrix}, \quad (24)$$

where the symbol \mathbf{A} indicates the in-plane stiffness matrix. \mathbf{B} and \mathbf{D} are the coupling stiffness and bending stiffness matrices. The superscripts I and T are related to the inelastic and thermal components.

3. Model Validation

The studied SMPC is prepared with T-700SC short carbon fibers and trans-1, 4-polyisoprene (TPI) matrix. The average length and diameter of the carbon fiber are 2 mm and $7 \mu\text{m}$, respectively. To verify the proposed method, the next two procedures are executed: (1) the ellipsoid fibers are assumed to be periodically distributed in the cubic matrix to equivalently replace the SMPC reinforced with natural short fibers. On this basis, a RVE with the ellipsoid inclusion can be easily selected, which can be easily discretized by the hexahedral subcells as shown in Figure 2(c). Moreover, its elastic modulus is calculated by the HFGMC and the FEM for a comparison. (2) A novel modeling procedure is proposed to acquire effective property of the SMPC with respect to ambient temperature, and the numerical results are compared with the experimental data. The constituent material parameters of the T700SC inclusion and TPI matrix at room temperature, including elastic modulus and Poisson's ratio, are shown in Table 1.

3.1. A Comparison between Numerical Methods. To validate effectiveness of the microscopic mechanical theory, a sphere inclusion whose center coincides with the cubic RVE is considered. Figure 3 indicates the elastic modulus of the composites with respect to fiber volume fraction (FVF). For a comparison, numerical results by the FEM are also indicated in the figure when the FVFs are 0.2 and 0.3. It should be pointed out that the identical subcell number $30 \times 30 \times 30$ are used to discretize the RVE during the numerical modeling. It can be easily found that the numerical results by the 3D HFGMC exhibit a good consistency with the FEM. In addition, it can be easily discerned that the elastic modulus exhibit an exponential growth with the variation of the FVF. In details, elastic modulus is 87.7 MPa when the FVF = 0.2 is considered, while the elastic modulus approximate to 478.8 MPa and 793.2 MPa when the FVF are 0.48 and 0.5, respectively.

TABLE 1: Constituent material parameters.

Constituent materials	Elastic modulus (MPa)	Poisson's ratio
T-700SC	230×10^3	0.307
TPI	54.2	0.35

To further investigate the inclusion shape influences on the elastic modulus, axial length of the ellipsoid inclusion is investigated. Herein, the RVE dimension of $d : h : l = 2 : 1 : 1$ and the FVF = 0.2 are considered in the example. The parameters d , h , and l denote the dimension of the RVE along y_1 -, y_2 -, and y_3 -direction as shown in Figure 2(c), respectively. It can be easily found from Figure 4 that longitudinal and transverse modulus represented a nonlinear variation with respect to axial length ratio of the ellipsoid inclusion. Moreover, transverse modulus exhibits a sharp decrease with an increase of the axial length ratio. In details, the transverse modulus is approximate to 105.1 MPa when the ellipsoid inclusion dimension $d_s : h_s : l_s = 1.2 : 1 : 1$ is determined. It should be pointed out that the parameters d_s , h_s , and l_s denote the ellipsoid fiber dimension. However, the transverse modulus is equal to 85.1 MPa when the ellipsoid inclusion dimension $d_s : h_s : l_s = 2.6 : 1 : 1$ is considered. However, the longitudinal modulus is 81.3 MPa when the ellipsoid inclusion dimension $d_s : h_s : l_s = 1.2 : 1 : 1$ is considered.

3.2. A Comparison with the Experimental Data. It is reported by Cai et al. [31, 32] (2021, 2022) that the FVF long thickness exhibits an obvious difference. In other words, the fiber distributed in the UD lamina close to the laminate surface is relative fewer. Therefore, it is critical to determine the FVF in each UD lamina, which can be found in Table 2. Herein, the FVF of the SMPC from 5% to 9% are considered in the example. The SMPC is further divided into 10 UD laminas, and the FVF in the surface UD laminas is different. Herein, the symbol “#” indicates the lamina number along thickness direction as shown in Figure 2(b). In addition, the ellipsoid fiber content should also be determined. According to the experimental data at room temperature, the ellipsoid fiber dimension in the 5% SMPC is determined by $d_s : h_s : l_s = 2.6 : 1 : 1$. Elastic modulus at an elevated temperature is also considered in the example. Herein, it should be noted that the elastic modulus of matrix materials is temperature-dependent, whose material parameters are provided by Zeng et al. [42, 43]. It should be noted that Poisson's ratio of the constituent materials is considered to be temperature-independent. In other words, this parameter of the constituent materials is a constant without respect to the ambient temperature influence during the numerical calculation. With respect to the raised ambient temperature, a sharp decrease of the elastic modulus for the SMPC is easily discerned as shown in Figure 5. This is attributed to the decreased modulus of matrix materials. Moreover, numerical results represent a good consistency to the experimental data. Overall, numerical results by the presented method exhibit a higher accuracy than the method proposed by Zeng et al. [42]. In details, an approximate results between the

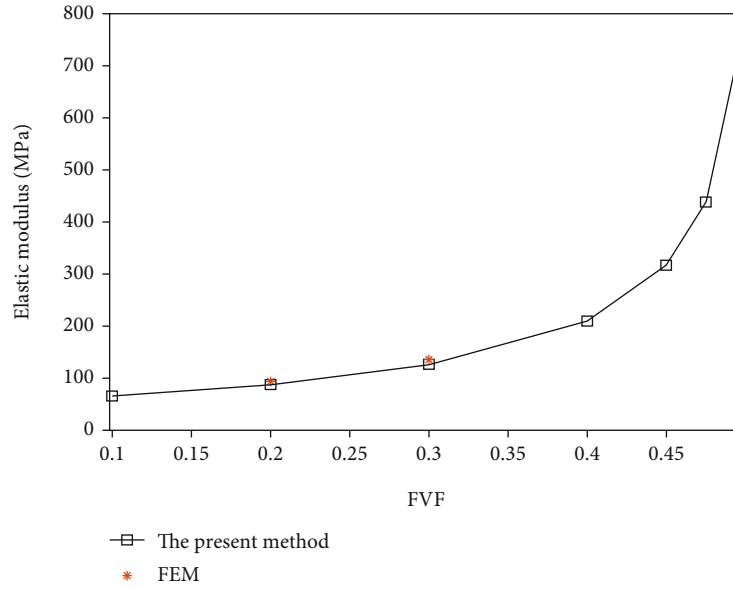


FIGURE 3: A comparison of elastic modulus E_{11} between the HFGMC and the FEM.

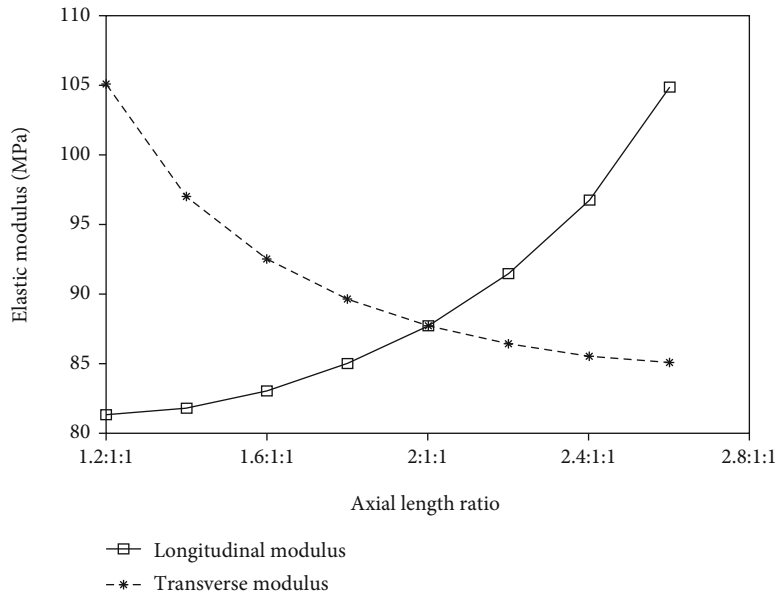


FIGURE 4: Elastic modulus investigation with respect to axial length ratio of the ellipsoid inclusion.

TABLE 2: FVF in each lamina.

FVF of the composites	1#	2#	3#	4#	5#	6#	7#	8#	9#	10#
5%	1%	6%	6%	6%	6%	6%	6%	6%	6%	1%
7%	3%	8%	8%	8%	8%	8%	8%	8%	8%	3%
9%	5%	10%	10%	10%	10%	10%	10%	10%	10%	5%

present method and the Zeng’s method can be found at 301 K. The maximum error can be found when the ambient temperature is equal to 334 K, and the present method exhibits a much higher accuracy than the method proposed by Zeng et al.

Similarly, procedures are also executed on the 7% and 9% SMPC to determine the ellipsoid fiber dimension at room temperature, and elastic modulus with respect to ambient temperature is also investigated as shown in Figures 6–7. The ellipsoid inclusion dimension are $d_s : h_s$

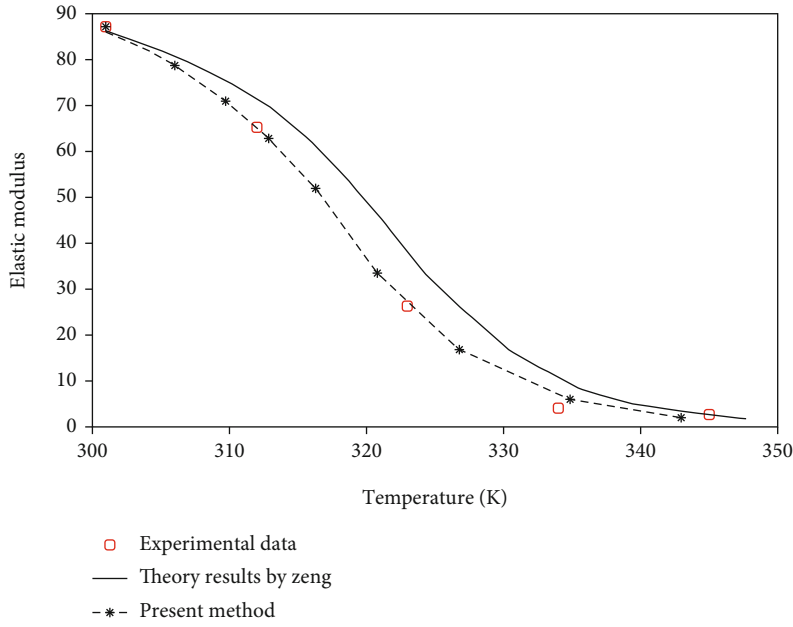


FIGURE 5: A comparison of elastic modulus with respect to ambient temperature when the FVF = 5%.

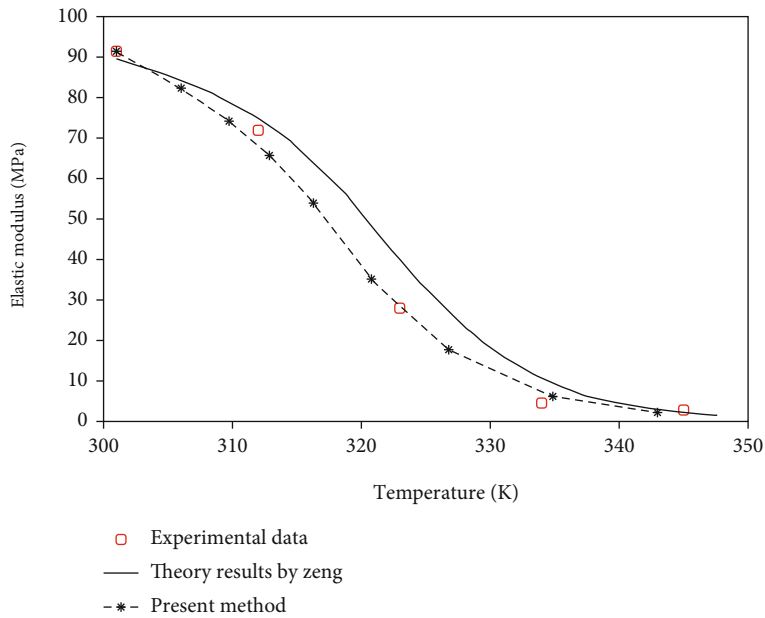


FIGURE 6: A comparison of elastic modulus with respect to ambient temperature when the FVF = 7%.

: $l_s = 2.4 : 1 : 1$ and $d_s : h_s : l_s = 2.1 : 1 : 1$, respectively. Combing with the FVF = 5%, an obvious difference of the inclusion dimension can be found. A sharp decrease of elastic modulus can be found when a higher ambient temperature is considered. Compared with experimental data, it is revealed that numerical results provided by the present method exhibit a higher accuracy than the theoretical method provided by Zeng et al. [42]. Combined with the numerical results as shown in Figures 4–6, it can be concluded that the FVF will contribute to an increase of the elastic modulus. In details, the elastic modulus is approximate to 86.99 MPa at the room temperature when the FVF = 5%.

While the elastic moduli increase to 91.12 MPa and 93.32 MPa when the FVF is 7% and 9%, respectively.

4. Failure Strength Investigations

It is critical for researchers to grasp the failure property of the SMPC in service to maximum their usage life. However, the failure characteristic are closely dependent on many factors, including the FVF, fiber arrangement, and constituent material property. In addition, the service environment also plays an important role in the mechanical property. For instance, the SMPC are exposed to a high temperature

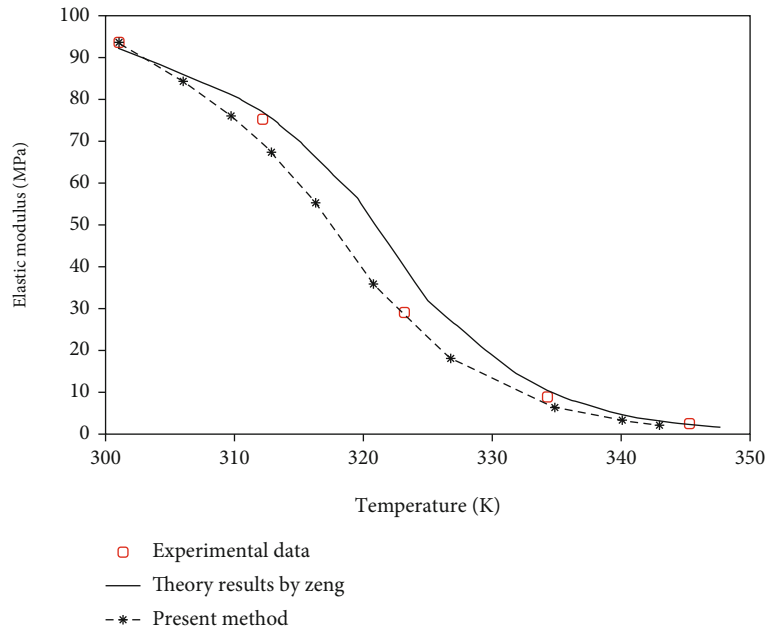


FIGURE 7: A comparison of elastic modulus with respect to ambient temperature when the FVF = 9%.

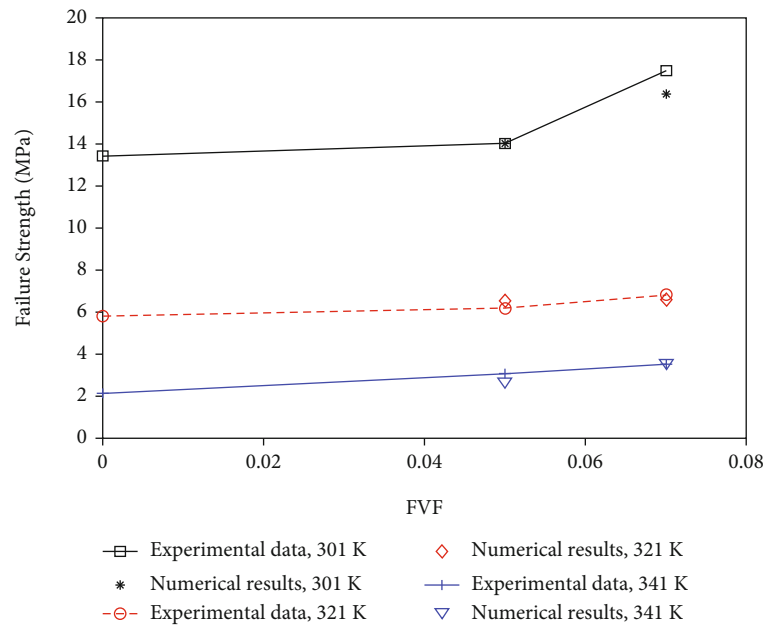


FIGURE 8: Investigations of the failure strength with respect to the FVF variations at different ambient temperatures.

condition, which may seriously reduce the failure strength. To fully grasp ambient variation influences, the failure strength at the room temperature and the elevated temperatures 321 K and 341 K are considered. To further valuate the failure strength of the SMPC with respect to the FVF variations, the SMP mixed with 5% and 7% natural short fibers are also investigated. It should be noted that the discretize mode of the composite laminate and inclusion shape in the matrix materials are identical with the study in Section 3. Moreover, the inelastic deformation derived from the matrix materials and thermal residual stress derived from the preparation process are both ignored.

Figure 8 indicates the failure strength of the SMPC with respect to the FVF variations at three ambient temperatures, that is, 301 K, 321 K, and 341 K. Herein, the failure property of the constituent materials at different ambient temperatures are derived from the study by Guo et al. [43]. The fiber longitudinal and transversal failure strengths are 4900 MPa and 80 MPa, respectively. During the prediction of the final failure strength, the maximum stress criterion [44] is employed. It should be pointed out that the failure strength of matrix is temperature-dependent, while the fiber strength always equal to a constant in evaluating the final failure strength at different ambient temperatures. For a further

validation, experimental data and numerical results of the failure strength are both indicated. In general, a good consistency between numerical results and experimental data can be found in the figure, and the increased short fibers tend to improve the failure strength of the SMPC in some extent. This is attributed to a higher failure strength of the natural fibers. The maximum error 6.34% can be found under the 301 K when the FVF = 0.07 is considered. In addition, an elevated temperature tends to sharply decrease the final failure strength of the SMPC. In details, the failure strength is approximate to 16.39 MPa when the ambient temperature 301 K is considered. However, the failure strengths decreased to 6.61 MPa and 3.59 MPa when the ambient temperatures 321 K and 341 K are considered. This is attribute to a huge reduction of the elastic modulus with an increase of the ambient temperature. In other words, the lower elastic modulus of the constituent materials sharply decrease the stiffness behavior of the SMPC. Naturally, their failure strength is reduced to some extent.

5. Conclusions

In this study, mechanical behaviors of the SMPC reinforced with natural short fibers were investigated by the presented constitutive model. The SMPC represents a huge deformation in service, and the improved laminate theory is suitable to describing its deformation and inclusion fraction influences on the SMPC. Numerical results of the elastic constants show a good consistency with the experimental data, which demonstrated the improved constitutive model. The conclusions are summarized as follows:

- (1) The SMPC reinforced with natural short fibers can be considered as the composite laminates, which are composed of the UD laminas with ellipsoid inclusion, whose inclusion dimension can be easily determined according to the experimental data at room temperature
- (2) The present method exhibits a good accuracy in investigating elastic modulus, which represents a sharp decrease with respect to an elevate temperature. For the 5% SMPC, the ellipsoid fiber dimension $d_s : h_s : l_s = 2.6 : 1 : 1$ represents a good consistency with experimental data. When the SMPC with 7% and 9% short fibers are considered, the ellipsoid inclusion dimensions are $d_s : h_s : l_s = 2.4 : 1 : 1$ and $d_s : h_s : l_s = 2.1 : 1 : 1$, respectively
- (3) The final failure strength of the SMPC can be effectively acquired by the proposed ellipsoidal inclusion model, and a higher ambient temperature results in a sharp decrease of their failure strength

The investigations in this article provide a new rapid evaluation method in predicting the mechanical property of natural short fiber composites, while the proposed method limits to a small FVF. A higher FVF gives rise to a negative influence on the failure strength, which may be attributed to the variation of interfacial property.

Data Availability

The raw/processed data required to reproduce these findings cannot be shared at this time due to technical or time limitations.

Conflicts of Interest

The authors declare that they have no known competing financial interests or personal relationships that could have appeared to influence the work reported in this paper.

Authors' Contributions

Yang Li is responsible for writing—original draft and methodology; Junjie Ye for writing—original draft, methodology, and supervision; Lu Liu for validation, visualization, and software; Baoquan Shi for methodology, writing—review and editing, and supervision; and Yumin He for validation and visualization.

Acknowledgments

This work was supported by the National Natural Science Foundation of China, China (nos. 52175112 and 51675397); the National Natural Science Foundation of Shaanxi Province, China (no. 2018JM5029); and the Fundamental Research Funds for the Central Universities (JB210421).

References

- [1] E. Yarali, A. Taheri, and M. A. Baghani, "A comprehensive review on thermomechanical constitutive models for shape memory polymers," *Journal of Intelligent Material Systems and Structures*, vol. 31, no. 10, pp. 1243–1283, 2020.
- [2] S. Basak and A. Bandyopadhyay, "Solvent responsive shape memory polymers-evolution, current status, and future outlook," *Macromolecular Chemistry and Physics*, vol. 222, no. 19, article 2100195, 2021.
- [3] J. S. Leng, X. Lan, Y. J. Liu, and S. du, "Shape-memory polymers and their composites: stimulus methods and applications," *Progress in Materials Science*, vol. 56, no. 7, pp. 1077–1135, 2011.
- [4] P. Mather, X. Luo, and I. Rousseau, "Shape memory polymer research," *Annual Review of Materials Research*, vol. 39, no. 1, pp. 445–471, 2009.
- [5] L. Xia, H. Gao, W. Bi, W. Fu, G. Qiu, and Z. Xin, "Shape memory behavior of carbon black-reinforced trans-1,4-polyisoprene and low-density polyethylene composites," *Polymers*, vol. 11, no. 5, 2019.
- [6] J. F. Castet and J. H. Saleh, "Satellite and satellite subsystems reliability: statistical data analysis and modeling," *Reliability Engineering and System Safety*, vol. 94, no. 11, pp. 1718–1728, 2009.
- [7] E. R. Abrahamson, M. S. Lake, N. A. Munshi, and K. Gall, "Shape memory mechanics of an elastic memory composite resin," *Journal of Intelligent Material Systems and Structures*, vol. 14, no. 10, pp. 623–632, 2003.
- [8] J. Sun, Y. Y. Liu, and J. S. Leng, "Mechanical properties of shape memory polymer composites enhanced by elastic fibers

- and their application in variable stiffness morphing skins,” *Journal of Intelligent Material Systems and Structures*, vol. 26, no. 15, pp. 2020–2027, 2014.
- [9] Y. An, J. Kim, N. S. Goo et al., “Preparation and analysis of the deployment behavior of shape memory polymer composite antennas,” *Composites Research*, vol. 31, no. 6, pp. 347–354, 2018.
- [10] M. S. Murugan, S. Rao, and G. N. Dayananda, “Actuation of shape memory polymer composites triggered by electrical resistive heating,” *Journal of Intelligent Material Systems and Structures*, vol. 28, no. 17, pp. 2363–2371, 2017.
- [11] L. Xia, X. Liu, and Z. Huang, “Study of electro-induced shape-memory *Eucommia ulmoides* rubber composites reinforced with conductive carbon blacks,” *Express Polymer Letters*, vol. 15, no. 7, pp. 600–611, 2021.
- [12] K. Yu, Y. J. Liu, and J. S. Leng, “Conductive shape memory polymer composite incorporated with hybrid fillers: electrical, mechanical, and shape memory properties,” *Journal of Intelligent Material Systems and Structures*, vol. 22, no. 4, pp. 369–379, 2011.
- [13] A. Basit, G. L’Hostis, and B. Durand, “The recovery properties under load of shape memory polymer composite material,” *Materials Science and Engineering Technology*, vol. 50, no. 12, pp. 1555–1559, 2020.
- [14] V. L. Le and N. S. Goo, “Deployment performance of shape memory polymer composite hinges at low temperature,” *Journal of Intelligent Material Systems and Structures*, vol. 30, no. 17, pp. 2625–2638, 2019.
- [15] Z. Q. Wang, J. B. Liu, J. M. Guo, X. Sun, and L. Xu, “The study of thermal, mechanical and shape memory properties of chopped carbon fiber-reinforced TPI shape memory polymer composites,” *Polymers*, vol. 9, no. 11, pp. 594–604, 2017.
- [16] T. D. Dao, N. S. Goo, and W. R. Yu, “Blocking force measurement of shape memory polymer composite hinges for space deployable structures,” *Journal of Intelligent Material Systems and Structures*, vol. 29, no. 18, pp. 3667–3678, 2018.
- [17] T. D. Dao, N. S. Goo, and W. R. Yu, “Design, fabrication, and bending test of shape memory polymer composite hinges for space deployable structures,” *Journal of Intelligent Material Systems and Structures*, vol. 29, no. 8, pp. 1560–1574, 2017.
- [18] B. D. Annin, E. V. Karpov, and A. Y. Larichkin, “Influence of anisotropy on the deformation of a polymer composite with shape memory,” *Mechanics of Solids*, vol. 55, no. 6, pp. 761–766, 2020.
- [19] C. Lelieveld, K. Jansen, and P. Teuffel, “Mechanical characterization of a shape morphing smart composite with embedded shape memory alloys in a shape memory polymer matrix,” *Journal of Intelligent Material Systems and Structures*, vol. 27, no. 15, pp. 2038–2048, 2016.
- [20] M. Kim, S. Jang, S. Choi, J. Yang, J. Kim, and D. Choi, “Analysis of shape memory behavior and mechanical properties of shape memory polymer composites using thermal conductive fillers,” *Micromachines*, vol. 12, no. 9, article 1107, 2021.
- [21] X. Z. Xin, L. W. Liu, Y. J. Liu, and J. Leng, “Mechanical models, structures, and applications of shape-memory polymers and their composites,” *Acta Mechanica Solida Sinica*, vol. 32, no. 5, pp. 535–565, 2019.
- [22] Z. Q. Wang, M. Z. Chang, F. Y. Kong, and K. Yun, “Optimization of thermo-mechanical properties of shape memory polymer composites based on a network model,” *Chemical Engineering Science*, vol. 207, pp. 1017–1029, 2019.
- [23] A. I. Arvanitakis, “A constitutive level-set model for shape memory polymers and shape memory polymeric composites,” *Archive of Applied Mechanics*, vol. 89, no. 9, pp. 1939–1951, 2019.
- [24] J. P. Gu, H. Y. Sun, H. Zeng, and Z. Cai, “Modeling the thermomechanical behavior of carbon fiber-reinforced shape memory polymer composites under the finite deformation,” *Journal of Intelligent Material Systems and Structures*, vol. 31, no. 4, pp. 503–514, 2020.
- [25] H. Y. Sun, J. P. Gu, Y. Tang, and Z. M. Xie, “Multi-scale analysis of thermo-mechanical properties of 2.5d angle-interlock woven shape memory polymer composites,” *Journal of Mechanics*, vol. 35, no. 4, pp. 475–486, 2019.
- [26] D. Bergman and B. Yang, “An analytical shape memory polymer composite beam model for space applications,” *International Journal of Structural Stability and Dynamics*, vol. 16, no. 2, article 1450093, 2016.
- [27] F. Li, L. Liu, X. Lan et al., “Modal analyses of deployable truss structures based on shape memory polymer composites,” *International Journal of Applied Mechanics*, vol. 8, no. 7, article 1640009, 2017.
- [28] J. J. Song, Q. Chen, and H. E. Naguib, “Constitutive modeling and experimental validation of the thermo-mechanical response of a shape memory composite containing shape memory alloy fibers and shape memory polymer matrix,” *Journal of Intelligent Material Systems and Structures*, vol. 27, no. 5, pp. 625–641, 2016.
- [29] S. M. R. Khalili, A. Saeedi, and E. Fakhimi, “Evaluation of the effective mechanical properties of shape memory wires/epoxy composites using representative volume element,” *Journal of Composite Materials*, vol. 50, no. 13, pp. 1761–1770, 2016.
- [30] N. Liu and L. L. Jiang, “Effect of microstructural features on the thermal conducting behavior of carbon nanofiber-reinforced styrene-based shape memory polymer composites,” *Journal of Intelligent Material Systems and Structures*, vol. 31, no. 14, pp. 1716–1730, 2020.
- [31] H. Cai, J. Ye, J. Shi et al., “A new two-step modeling strategy of the randomly distributed short fibers in composites with respect to primary voids,” *Composite Science and Technology*, vol. 218, article 109122, 2022.
- [32] H. Cai, J. J. Ye, J. W. Y. W. Wang et al., “An effective micro-scale approach for determining the anisotropy of polymer composites reinforced with randomly distributed short fibers,” *Composite Structures*, vol. 240, article 112087, 2020.
- [33] S. Lurie, D. Volkov-Bogorodsky, and E. Aifantis, “Eshelby’s inclusion problem in the gradient theory of elasticity: applications to composite materials,” *International Journal of Engineering Science*, vol. 49, no. 12, pp. 1517–1525, 2011.
- [34] M. Katouzian and S. Vlase, “Mori-Tanaka formalism-based method used to estimate the viscoelastic parameters of laminated composites dagger,” *Polymers*, vol. 12, no. 11, article 2481, 2020.
- [35] R. B. Yang, Y. M. Lee, Y. C. Shiah, and T. W. Tsai, “On the generalized self-consistent model for the effective thermal conductivity of composites reinforced by multi-layered orthotropic fibers,” *International Communications in Heat and Mass Transfer*, vol. 49, pp. 55–59, 2013.
- [36] J. Aboudi, S. M. Arnold, and B. A. Bednarczyk, *Micromechanics Software*, Elsevier Science Pub. Ltd, Amsterdam, Netherlands, 2013.

- [37] J. J. Ye, Y. W. Wang, Z. W. Li et al., "Failure analysis of fiber-reinforced composites subjected to coupled thermo-mechanical loading," *Composite Structures*, vol. 235, article 111756, 2020.
- [38] J. J. Ye, C. C. Chu, H. Cai et al., "A multi-scale model for studying failure mechanisms of composite wind turbine blades," *Composite Structures*, vol. 212, pp. 220–229, 2019.
- [39] J. Aboudi and M. Ryvkin, "The effect of localized damage on the behavior of composites with periodic microstructure," *International Journal of Engineering Science*, vol. 52, pp. 41–55, 2012.
- [40] G. L. Shen, G. K. Hu, and B. Liu, *Mechanics of Composite Materials*, Tsinghua University Press, China, 2013.
- [41] Z. Zhai, *Multiscale Modeling Based on Generalized Cell of Method and Its Application in Composite Structural Health Monitoring*, [Ph.D. Thesis], Xi'an Jiaotong University, China, 2014.
- [42] H. Zeng, J. Leng, J. Gu, and H. Sun, "Modeling the thermomechanical behaviors of short fiber reinforced shape memory polymer composites," *International Journal of Mechanical Sciences*, vol. 166, article 105212, 2020.
- [43] J. Guo, Z. Wang, L. Tong, H. Lv, and W. Liang, "Shape memory and thermo-mechanical properties of shape memory polymer/carbon fiber composites," *Composites: Part A*, vol. 76, pp. 162–171, 2015.
- [44] Y. Wang, *Mechanics and Structural Design of Composite Materials*, East China University of science and technology Press, Shanghai, 2012.